WATER RESOURCES RESEARCH, VOL. 49, 4775–4791, doi:10.1002/wrcr.20303, 2013

Detailed simulation of morphodynamics: 2. Sediment pickup, transport, and deposition

M. Nabi,[1] H. J. de Vriend,[2,3] E. Mosselman,[2,3] C. J. Sloff,[2,3] and Y. Shimizu[1]

Received 26 January 2012; revised 30 April 2013; accepted 5 May 2013; published 7 August 2013.

[1] The paper describes a numerical model for simulating sediment transport with eddy-resolving 3-D models. This sediment model consists of four submodels: pickup, transport over the bed, transport in the water column and deposition, all based on a turbulent flow model using large-eddy simulation. The sediment is considered as uniform rigid spherical particles. This is usually a valid assumption for sand-bed rivers where underwater dune formation is most prominent. Under certain shear stress conditions, these particles are picked up from the bed due to an imbalance of gravity and flow forces. They either roll and slide on the bed in a sheet of sediment or separate from the bed and get suspended in the flow. Sooner or later, the suspended particles settle on the bed again. Each of these steps is modeled separately, yielding a physics-based process model for sediment transport, suitable for the simulation of bed morphodynamics. The sediment model is validated with theoretical findings such as the Rouse profile as well as with empirical relations of sediment bed load and suspended load transport. The current model shows good agreement with these theoretical and empirical relations. Moreover, the saltation mechanism is simulated, and the average saltation length, height, and velocity are found to be in good agreement with experimental results.

Citation: Nabi, M., H. J. de Vriend, E. Mosselman, C. J. Sloff, and Y. Shimizu (2013), Detailed simulation of morphodynamics: 2. Sediment pickup, transport, and deposition, *Water Resour. Res.*, *49*, 4775–4791, doi:10.1002/wrcr.20303.

1. Introduction

[2] Morphology is the consequence of sediment transport and sedimentation in the river [*Church*, 2006], and therefore, the formation of morphological structures without sediment is not possible. The formation of ripples, dunes, bars, and other alluvial features are governed by flow-induced sediment motion, the structure of the bed, and sediment-bed interactions. Given the small particle size, turbulence at Kolmogorov scales is relevant to sediment motion. The lack of accurate physics-based models of sediment transport at these scales makes the prediction of small-scale alluvial processes such as ripples and dunes formation difficult. Rolling and saltation of sediment grains over the bed in turbulent flow are inherently complex problems. Turbulence produces near-bed velocities and pressure fluctuations that give rise to fluctuations in the forces on sediment particles, due to which sediment may be picked up and transported by the fluid. On the other hand, the presence of sediment particles in the flow may generate or suppress turbulence, thus creating a dynamic feedback system [*Bridge and Best*, 1998].

[3] In the past, sediment transport has mainly been described in terms of bulk fluxes related to mean flow properties. Some of these sediment transport formulae include a threshold of motion expressed in terms of a critical shear stress following *Shields* [1936]. *Wiberg and Smith* [1987], *Dey* [1999], and *Wu and Chou* [2003] addressed the issue of incipient motion as a function of the mean bed shear stress via a deterministic analysis of noncohesive sediment particles on a loose sediment bed. In contrast to this deterministic view, the stochastic view is that turbulent stress variations are responsible for the initial dislodgment of sediment. *Einstein and El-Samni* [1949], *Nelson et al*. [1995], and *Papanicolaou et al*. [2002] dealt with sediment entrainment based on stochastic approaches.

[4] *Schmeeckle and Nelson* [2003] applied direct numerical simulation (DNS) for bed-load transport. The difficulty arising in this kind of simulations is how to define the lift force applied on the sediment particles. The phenomenon of particle lift is still not completely understood and adequate experimental results are not available to determine a reliable quantitative relationship. *Saffman* [1965] considered the lift force on a small sphere in an unbounded, linear shear flow. He assumed that the particle and shear Reynolds numbers are much smaller than unity and that the particle Reynolds number is much smaller than the shear Reynolds number. *Harper and Chang* [1968] extended

Companion paper to *Nabi et al.* [2012] doi:10.1029/2012WR011911 and *Nabi et al.* [2013] doi: 10.1002/wrcr.20457.

[1]Laboratory of Hydraulic Research, Hokkaido University, Sapporo, Japan.
[2]Section of Hydraulic Engineering, Delft University of Technology, Delft, Netherlands.
[3]Department of River Dynamics, Morphology & Water Transport, Deltares, Delft, Netherlands.

Corresponding author: M. Nabi, Laboratory of Hydraulic Research, Graduate School of Engineering, Hokkaido University, Sapporo, Japan. (M.Nabi@eng.hokudai.ac.jp)

0043-1397/13/10.1002/wrcr.20303

Saffman's analysis to arbitrary three-dimensional bodies in linear shear flow. *Drew* [1978] performed a similar analysis for a small sphere in two-dimensional strain flow. *McLaughlin* [1991] extended Saffman's analysis to situations in which the particle Reynolds number is not necessarily small compared to the shear Reynolds number. *Kurose and Komori* [1999] studied the lift and drag forces on a rotating sphere in a linear shear flow. They applied DNS and investigated the effects of both shear and rotational speed on the drag and lift forces for particle Reynolds numbers $1 \leq Re_p \leq 500$. They showed that their DNS results are in good agreement with McLaughlin's results.

[5] *Dey* [1999] presented a model to compute the threshold shear stress for noncohesive nonuniform sediment motion on a horizontal sedimentary bed, under a unidirectional steady uniform stream flow. This work was extended by *Dey and Debnath* [2000] for a horizontal and streamwise sloping sediment bed. Experimental data on thresholds of sediment motion were used to calibrate their model, using the lift coefficient as a free parameter. *McEwan and Heald* [2001] examined the stability of randomly deposited sediment beds using a discrete particle model in which individual grains were represented by spheres. The results indicated that the threshold shear stress for flat beds consisting of cohesionless uniformly sized grains cannot be adequately described by a single-valued parameter; rather, it is best represented by a distribution of values. *Papanicolaou et al*. [2002] conducted theoretical studies on the stochastic aspect of the problem of incipient motion. They showed that the sediment transport may be underpredicted if the incipient motion criteria are based exclusively on time-averaged bed shear stress. Moreover, they investigated the role of near-bed turbulent fluctuations and bed packing density on incipient sediment motion. *Wu and Chou* [2003] incorporated the probabilistic features of the turbulent fluctuations and bed grain geometry and investigated the rolling and lifting probabilities for sediment entrainment. They extended the theoretical formulation of the entrainment probabilities in smooth-bed flows by using the lognormally distributed instantaneous velocity and uniformly distributed initial grain position, along with a relation between lift coefficient and particle Reynolds number. Their results show that a reliable probability for the critical state of sediment entrainment cannot be found.

[6] A notable study of particle motion was conducted by *Escauriaza and Sotiropoulos* [2011]. They carried out a numerical study of particle motion in a Lagrangian framework. They initially placed a number of spherical particles on the bed upstream of a vertically mounted circular cylinder in a rectangular open channel. The detached-eddy simulation (DES) approach was used to simulate the flow field. The trajectory and momentum equations for the sediment particles were solved simultaneously with the flow equations, assuming one-way coupling between sediment and flow, and neglecting particle-to-particle interactions. Their computed results show that the transport of particles is highly intermittent and exhibits fundamentally all the features of bed-load sediment transport observed in laboratory experiments and field measurements.

[7] In most of the existing models for sediment motion, a mean bed shear stress is applied. The velocity distribution is considered to follow a logarithmic profile and the effect of turbulent structures, as well as fluctuations, on sediment motion is implicit. Moreover, even if the flow part of the model is solved accurately, the sediment motion mechanism is not solved completely, and the interaction of sediment (pickup and deposition) with the bed is not taken into account. The deficiency of the existing sediment models is the reason to develop a sediment model in which all stages of motion and their effect on the bed morphodynamics are considered.

[8] We developed a high-resolution 3-D numerical model for morphodynamic processes on small temporal and spatial scales, based on large-eddy simulation, particle-based transport of sediment, and adaptation of the computational domain to bed level changes by means of adaptive grid refinement and immersed boundary techniques. In this paper, we present the model for sediment motion, which consists of submodels for pickup, transport over the bed, transport in the water column, and deposition. The sediment is modeled in a deterministic way considering the sediment as rigid spherical particles in the turbulent flow. Depending on the shear stresses, the particles roll and slide as a sheet layer over the bed or separate from the bed while jumping or being suspended by the flow. We test the sediment model against well-established analytical and empirical relations. We find that the model correctly reproduces the settling velocity of a single particle in stagnant water, the angle of repose after avalanching, and the Rouse profile for the concentration of suspended sediments. Computed sediment transport rates are within the range of values predicted by empirical transport formulae and agree in particular with the formulae of *Meyer-Peter and Müller* [1948] and *Wiberg and Smith* [1987]. Furthermore, the average saltation length, height, and velocity are calculated, and a good agreement is found with the results of *Niño and García* [1998].

[9] We applied the model to uniform small spherical particles, which is a suitable approximation for sand beds where the random orientation of the particles leads to an averaged spherical form. This approximation may not be true for gravel beds, because the larger elliptical particles of these beds develop a preferential orientation, depending on the stage of armoring [*Allen*, 1982].

[10] Two companion papers present the methods and the validation of the underlying hydrodynamic model [*Nabi et al*., 2012] and the associated model for changes in bed level as a result of sediment pickup, transport, and deposition (M. Nabi et al., Detailed simulation of morphodynamics: 3. Ripples and dunes, submitted to Water Resources Research, 2013).

2. Model Description

[11] The model for the sediment motion consists of four submodels, namely, pickup, transport over the bed, transport in the water column, and deposition. If the force on a particle, exerted by the flow and gravitation forces, exceeds a critical value, the particle moves. The particle either goes in suspension or rolls or slides on the bed. In the case of suspension, the particle may interact with the bed again after deposition. This interaction can take two forms: either the particle stays on the bed (viscous damping) or separates from the bed again (elastic rebounding). Each of the four submodels relates the motion of sediment to exerted forces

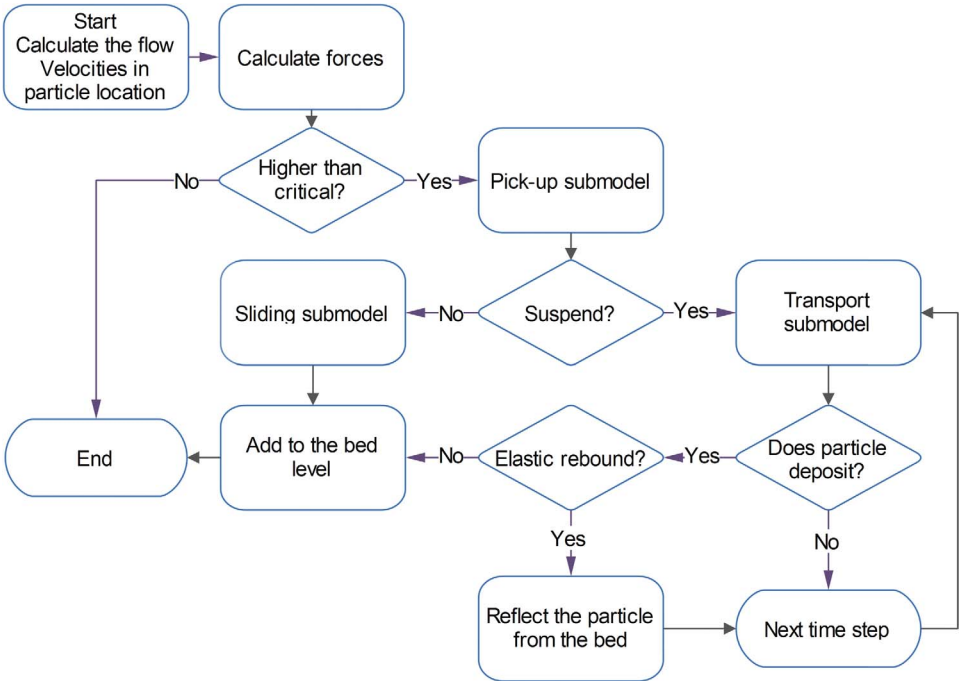

Figure 1. Flowchart of algorithms to simulate the motion of a single sediment particle.

and geometrical properties. Figure 1 shows a flowchart of the applied algorithms for a single particle. In section 3, we explain the forces exerted on a spherical particle, and in section 4, we explain the four submodels of sediment motion, considering the geometrical properties.

3. Forces on a Single Particle

[12] A particle immersed in a fluid is subject to gravity and fluid forces. In the next sections, these forces are formulated.

3.1. Drag Force

[13] The drag force is caused by the pressure gradient and viscous skin friction. As both are proportional to the relative flow velocity squared, the drag force for a spherical particle can be expressed as [*Michaelides*, 2006]

$$\vec{F}_{drag} = C_D \frac{\pi}{8} d^2 \rho (\vec{u}_f - \vec{v}_p)|\vec{u}_f - \vec{v}_p| \tag{1}$$

where ρ is the mass density of the fluid, d is the particle diameter, C_D is the drag coefficient, $\vec{v}_p$ is the particle velocity, and $\vec{u}_f$ is the flow velocity in the center of the particle, if the particle would be absent. *Morsi and Alexander* [1972] conducted an experimental study to investigate the relation between the drag coefficient C_D and the particle Reynolds number $\mathrm{Re}_p \left(\mathrm{Re}_p = |\vec{u}_f - \vec{v}_p| d/\nu\right)$, with ν denoting the kinematic viscosity. Their experiments showed that C_D can be approximated as a function of particle Reynolds number only. *Kurose and Komori* [1999] showed the drag force to be a function of the Reynolds particle number and the particle rotation speed. They showed that the effect of the rotation speed on the drag force is relatively small; therefore, we neglect it in the present study. We adopt the empirical equation for the drag coefficient, C_D, for a spherical particle proposed by *Morsi and Alexander* [1972]

$$C_D = a_0 + \frac{a_1}{Re_p} + \frac{a_2}{Re_p^2} \tag{2}$$

where a_0, a_1, and a_2 are coefficients dependent on Re_p. The values of a_0, a_1, and a_2 for a range of particle Reynolds numbers are given in *Morsi and Alexander* [1972].

3.2. Lift Force

[14] *Rubinow and Keller* [1961] and *Saffman* [1965] used matched asymptotic expansions to analyse the lift force acting on a rotating sphere in a linear unbounded shear flow with particle Reynolds numbers much lower than unity. Saffman's expression for the lift force coefficient $C_{L,Sa}$ on a sphere is given by

$$C_{L,Sa} = \frac{12.92}{\pi} \varepsilon \tag{3}$$

where ε represents the ratio of the square root of the shear Reynolds number to the particle Reynolds number, which is restricted to large values in Saffman's analysis $(\varepsilon \gg 1)$. *McLaughlin* [1991] extended Saffman's analysis to remove the restriction given to large values of ε. *Mei* [1992] obtained the following relation from McLaughlin's results.

$$\frac{C_L}{C_{L,Sa}} = 0.443J \tag{4}$$

where C_L is the lift coefficient and J is a nondimensional quantity arising from integration in McLaughlin's analysis. The lift force F_{lift} can be determined as

$$\vec{F}_{lift} = C_L \frac{\pi}{8} d^2 \rho |\vec{u}_f - \vec{v}_p|^2 \quad (5)$$

[15] Saffman's result is obtained for $J = 2.225$. *Mei* [1992] fitted a curve through the data from the table in *McLaughlin* [1991] to obtain a relation for J for $0.1 \leq \varepsilon \leq 20$:

$$J = J(\varepsilon) \approx 0.6765\{1 + \tanh[2.5\log_{10}(\varepsilon + 0.191)]\} \{0.667 + \tanh[6(\varepsilon - 0.32)]\} \quad (6)$$

[16] Moreover, the DNS results of *Kurose and Komori* [1999] for the lift force are in good agreement with those obtained by *McLaughlin* [1991]. In the present study, we apply McLaughlin's results (Mei's relations) to estimate the lift force on a sediment particle.

3.3. Submerged Weight

[17] Gravity and buoyancy forces are of major importance to the motion of sediment particles. Gravity and buoyancy forces have opposite directions, and their sum constitutes the submerged weight. The submerged weight of a spherical particle is given by

$$\vec{F}_G = \frac{\pi}{6} d^3 \left(\rho_p - \rho\right) \vec{g} \quad (7)$$

where ρ_p is the density of the sediment and $\vec{g}$ is the gravitational acceleration.

3.4. Other Forces

[18] More forces, such as added mass and Basset forces, affect particle motion. Because a particle and a fluid cannot exist in the same physical space simultaneously, the particle, no matter it is accelerating or decelerating, must repel some amount of surrounding fluid to pass through. Therefore, added mass or virtual mass is added to the particle to account for the corresponding inertia. To demonstrate this in a simplified model, some volume of a moving fluid with a moving particle can be used. The added mass force can be calculated by [*Auton*, 1987]

$$\vec{F}_{add} = C_m \rho V_p \left(\frac{D\vec{u}_f}{Dt} - \frac{d\vec{v}_p}{dt}\right) \quad (8)$$

where V_p is the volume of the particle and C_m is the added mass coefficient equal to 0.5 for spherical particles [*Auton*, 1987].

[19] The Basset force results from interaction of the particle with its own wake. The Basset force is often relatively small [*Armenio and Fiorotto*, 2001]; therefore, it is neglected in the present study.

4. Submodels for Sediment Movement

[20] We developed submodels for pickup, transport in the water column, deposition, and transport over the bed. We explain these four submodels of sediment motion in the next sections.

4.1. Sediment Pickup

[21] A sand bed can be approximated by interlocking layers of spherical particles. If the shear stress of the flow on the bed exceeds a certain value, the particles begin to rotate and may move from their positions. This stress level is called the critical shear stress, and the initiation of motion of particles is called incipient motion.

[22] Figure 2 shows the bed schematically. Each individual spherical particle is resting on three other closely packed spherical particles. It is the most stable three-dimensional configuration for spherical particles [*Dey*, 1999]. All particles are assumed to have the same size. Depending on the orientation of the three bed particles with respect to the direction of exerted forces, the solitary particle tends to roll either over the valley between two supporting particles, over the summit of a single particle or somewhere in between.

[23] The incipient motion of a spherical sediment particle is determined by the resultant of the forces acting on the particle as shown in Figure 3. The submerged weight always acts in the downward direction. The drag force is parallel to the flow direction, and the lift force is in the direction normal to the bed at the pickup point. The motion of spherical particles begins mostly by rolling, sometimes by sliding. For simplicity, incipient motion by sliding is ignored.

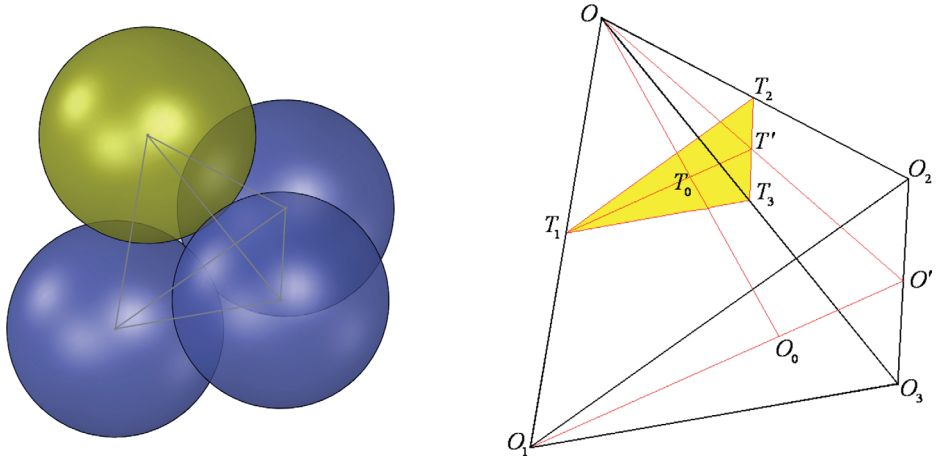

Figure 2. The configuration of an individual particle on the (left) three packed bed particles and a tetrahedron formed joining the (right) centers of the four particles.

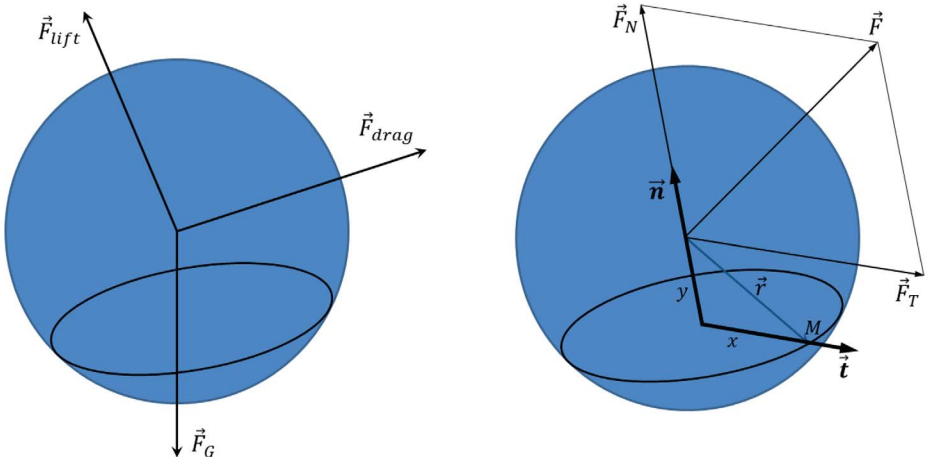

Figure 3. Forces on an individual particle exerted by (left) fluid and gravity and the projection of the total force on (right) normal and tangential directions.

[24] When a solitary particle is about to dislodge from its original position, the balance of moments about the point of contact M requires

$$\sum \vec{r} \times \vec{F} = 0 \tag{9}$$

or

$$F_n.x + F_t.y = 0 \tag{10}$$

where x and y are the tangential and normal lever arms, and F_t and F_n are magnitudes of the tangential and normal forces, respectively. The latter follow from

$$F_t = \vec{F}_{total}.\vec{t} \tag{11}$$

$$F_n = \vec{F}_{total}.\vec{n} \tag{12}$$

[25] Here $\vec{n}$ and $\vec{t}$ are the unit normal and tangential vectors. F_{total} is defined as the resultant of all acting forces $\left(\vec{F}_{total} = \vec{F}_G + \vec{F}_{drag} + \vec{F}_{lift}\right)$. By dividing F_t by the area of the particle, the exerted tangential particle shear stress τ can be found.

$$\tau = \frac{F_t}{2\pi d^2/4} \tag{13}$$

[26] The lever arms are determined according to Figure 2. T_1, T_2, and T_3 are the contact points of the three bed particles with the considered particle. The orientation of the acting forces determines whether this particle tends to roll over the valley, over the summit of a single particle, or somewhere in between. By considering the longest and shortest paths, the tangential lever arm will be

$$x_{min} = T_0T' = \frac{d}{4\sqrt{3}} \tag{14}$$

$$x_{max} = T_0T_1 = \frac{d}{2\sqrt{3}} \tag{15}$$

[27] A particle can choose different paths according to the direction of the acting forces. As the number of the exposed particles is very large, the average particle path corresponds with an average tangential lever arm of

$$x = \frac{x_{max} + x_{min}}{2} = \frac{\sqrt{3}}{8}d \tag{16}$$

[28] The normal lever arm y is equal to the distance between the center of the solitary particle and the plane $T_1T_2T_3$, which passes through the contact points. The normal lever arm y is not related to the direction of motion. By considering Figure 3, y can be found as

$$y = \frac{d}{\sqrt{6}} \tag{17}$$

[29] The acting point of moment changes its position during the rotation of the sphere. Figure 4 shows a particle during dislodge and rotation. The outer circles represent the physical geometry of the spheres, and the inner circles represent the effective averaged diameter from equations (16) and (17), equal to $2\sqrt{x^2+y^2}$. If φ is the angle of the tangential unit vector with the horizontal plane, the moment can be defined as

$$M = I\frac{\mathrm{d}^2\varphi}{\mathrm{d}t^2} \tag{18}$$

where I is the inertial moment; for a solid sphere, $I = md^2/10$. By projecting the forces on the line passing through the sphere centers and the line normal to it through the center of the moving sphere ($\vec{n}'$ and $\vec{t}'$ in Figure 4), the moment at point M can be written as

$$M = r.(F_t\sin\varphi + F_n\cos\varphi) \tag{19}$$

in which r is the radius of rotation $(r = \sqrt{x^2+y^2})$. Inserting equation (19) into equation (18) yields,

$$\frac{\mathrm{d}^2\varphi}{\mathrm{d}t^2} = A\sin\varphi + B\cos\varphi \tag{20}$$

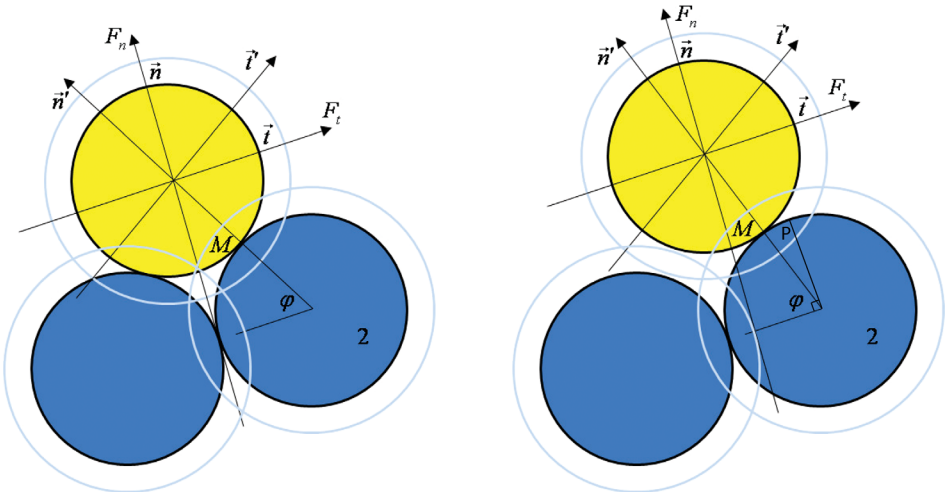

Figure 4. Presentation of forces and directions of the acting forces (left) before moving and (right) during incipient motion.

where

$$A = \frac{10F_t r}{md^2} \tag{21}$$

$$B = \frac{10F_n r}{md^2} \tag{22}$$

[30] Equation (20) is nonlinear and has no direct analytical solution, but it is possible to find a solution for $\mathrm{d}\varphi/\mathrm{d}t$, which can be considered as the radial velocity of the moving particle related to the center of the fixed particle. By applying the initial condition at $\varphi = \varphi_0$ as $\mathrm{d}\varphi/\mathrm{d}t|_{t=0} = 0$, this solution reads

$$\frac{\mathrm{d}\varphi}{\mathrm{d}t} = \sqrt{-2A(\cos\varphi - \cos\varphi_0) + 2B(\sin\varphi - \sin\varphi_0)} \tag{23}$$

[31] A complete dislodge of the sediment particle from the bed occurs when the rotating particle separates from the bed particle. In that case, the reaction force of particle 2 tends to zero. By projecting the tangential and normal forces on the line passing through the particle centers in Figure 4,

$$F_n \sin\varphi - F_t \cos\varphi = 0 \tag{24}$$

[32] Hence

$$\varphi = \tan^{-1}\left(\frac{F_t}{F_n}\right) \tag{25}$$

[33] As can be concluded from Figure 4, a particle separates from the bed if the angle of particle separation falls in the range of $\pi/3 \leq \varphi \leq 2\pi/3$. If the angle, φ, does not fall within this range, the particle cannot separate and will roll or slide along the bed. The model for transport over the bed will be discussed in section 4.4. We consider here the case in which $\pi/3 \leq \varphi \leq 2\pi/3$.

[34] By substituting φ into equation (23), the radial velocity can be found. The tangential velocity can be determined from:

$$v_{tan} = 2r\frac{\mathrm{d}\varphi}{\mathrm{d}t} \tag{26}$$

where v_{tan} is the particle velocity in the direction of $\vec{t}'$. The components of $\vec{v}_{tan}$ in x, y, and z directions will be the initial velocities of the particle at the moment of its pickup.

[35] Most existing formulations for pickup are empirical based on experimental data and lack rigorous theoretical description. The numerical simulation of the amount of pickup requires implementation of a discrete-element method (DEM) inside the bed which is computationally demanding. The huge computational costs in three-dimensional cases are the reason why we derive a parameterized formulation for the instantaneous pickup rate from the bed. According to this analysis, the particles are considered to be initially in rest. Due to lift and drag forces, the particles can accelerate. The acceleration is defined by a. To move over a distance equal to the grain diameter, d, a time $t = \sqrt{2d/a}$ is required. According to Newton's second law, the acceleration is the sum of the forces divided by the mass of the particle,

$$\vec{a} = \frac{\sum \vec{F}_{total}}{m_p} \tag{27}$$

where $\vec{F}_{total}$ is the resultant force on a single particle defined by $\vec{F}_{total} = \vec{F}_G + \vec{F}_{drag} + \vec{F}_{lift}$ and m_p is the mass of the particle. For uniform channel flow, the flow is determined by the friction velocity, u^*. Both the lift and drag forces can be expressed by the shear stress ($\tau_b = \rho u^{*2}$) as $\vec{F}_{lift} \sim \vec{\tau}_b d^2$ and $\vec{F}_{drag} \sim \vec{\tau}_b d^2$. The force balance can therefore be written as

$$\sum \vec{F} \sim d^2(\vec{\tau} - \vec{\tau}_{cr}) \tag{28}$$

where $\tau_{cr} \sim (\rho_p - \rho)gd$.

[36] From here on, we neglect the direction of the force, implying that we do not care about the direction of motion of the individual particle. As we are looking for the bulk quantity of bed entrainment, E, we consider a large number

of small spherical particles. The exact position of a single particle is therefore of minor importance. Then, the initial acceleration of the particle follows from

$$a \sim \frac{\sum F}{\rho_p d^3} = \frac{\tau - \tau_{cr}}{\rho_p d} = g\frac{\rho_p - \rho}{\rho_p}\left(\tau^* - \tau^*_{cr}\right) \tag{29}$$

where τ^* denotes the dimensionless shear stress, defined as

$$\tau^* = \frac{\tau}{\left(\rho_p - \rho\right)gd} \tag{30}$$

[37] Substitution of this acceleration into the timescale definition $t = \sqrt{2d/a}$ gives

$$t \sim \sqrt{\frac{\rho_p}{\rho_p - \rho}\frac{d}{\left(\tau^* - \tau^*_{cr}\right)g}} \tag{31}$$

[38] This means that the timescale is inversely proportional to the square root of the excess bed shear stress. The erosion rate then becomes

$$E \sim \rho_p \frac{d}{t} = \rho_p \sqrt{\frac{\rho_p - \rho}{\rho_p} gd\left(\tau^* - \tau^*_{cr}\right)} \tag{32}$$

or

$$E = \psi\rho_p \sqrt{\frac{\rho_p - \rho}{\rho_p} gd\left(\tau^* - \tau^*_{cr}\right)} \tag{33}$$

[39] The coefficient ψ is a tuning parameter and contains such factors as the packing of the bed and the shape of the particles. Equation (33) is similar to the pickup formula proposed by *De Ruiter* [1982, 1983] for uniform sediment, reading

$$E = \alpha_{Ruiter}\rho_p \mathcal{F}\left[\frac{\rho_p - \rho}{\rho_p} gd \frac{\tau^* - \tau^*_{cr}}{\tau^*_{cr}{}^0}\tan\phi\right]^{0.5} \tag{34}$$

in which $\mathcal{F}$ is a pickup probability function, $\tau^*_{cr}{}^0$ is the instantaneous critical shear stress at a horizontal bed, ϕ is the angle of repose, and α_{Ruiter} is a constant for uniform spherical particles. The angle of repose is constant. The critical shear stress at a horizontal bed can be determined by the balance of forces. The lift force can be neglected if it is small compared with the drag and gravity forces (which is not always true). Considering the drag parallel to the bed, and considering equations (16) and (17), the following balance of forces applies in the critical state:

$$F_{cr}\frac{d}{\sqrt{6}} = \left(\rho_p - \rho\right)\frac{\pi}{6}d^3 g\frac{\sqrt{3}}{8}d \tag{35}$$

[40] The particle shear stress is the acting force on a particle per unit effective surface area. The effective surface area is the projection of the particle surface in the direction of acting force, namely, $2(\pi d^2/4)$. Hence the critical particle shear stress is

$$\tau^*_{cr} = \frac{\tau_{cr}}{\left(\rho_p - \rho\right)dg} = \frac{\sqrt{2}}{8} \approx 0.177 \tag{36}$$

which means that the dimensionless critical particle shear stress for a flat bed is also constant. Note that the critical particle shear stress in the current model is generally not constant, but rather a function of the bed slope and the directions of the forces. Also note that the critical particle shear stress in equation (36) is not the same as the *Shields* [1936] critical shear stress. The Shields diagram is stochastic in its nature as it is based on the mean bed shear stress ($= \overline{\tau}/(\rho_p - \rho)dg$, where $\overline{\tau}$ is averaged bed shear stress) and it contains only a single line which separates the motion from no-motion conditions. The original diagram in the publication of *Shields* [1936] presents a range of values at which either motion or rest is possible. This stress is almost half the critical fluctuating shear stress, because the effect of turbulent velocity fluctuations is not taken into account. The peaks of the fluctuating shear stress amount to about twice the mean value [*De Ruiter*, 1982].

[41] We performed a large number of simulations with different bulk velocities and particle diameters and averaged the simulated particle shear stress over the bed area and compared the result with the mean bed shear stress (as used in Shields diagram). Figure 5 shows a comparison between the averaged simulated particle shear stress and the mean bed shear stress. We found a nearly linear relation between them. The constant of proportionality for this linear relation turns out to be independent of the bulk velocity and is only a function of the particle diameter. The best fit for this constant is found to be

$$\beta = 0.1855\left[\frac{\left(\rho_p/\rho - 1\right)gd^3}{36\nu^2}\right]^{0.1091} - 0.1043 \tag{37}$$

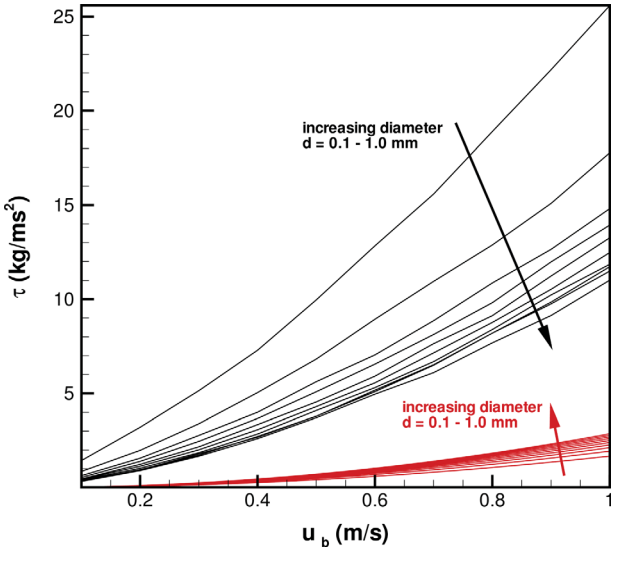

Figure 5. The averaged simulated particle shear stress (black) and Shields bed shear stress (red) for different particle diameters and bulk velocities.

[42] The linear relation between the mean bed shear stress and the mean particle shear stress implies that we can use equation (34) based on particles shear stress (for uniform sediment), since the ratio $(\tau^* - \tau^*_{cr})/\tau^{*0}_{cr}$ remains constant.

[43] According to *Van Rijn* [1984a], the constant in equation (34) is equal to 0.016. This value of α_{Ruiter} has been derived from experiments and is particularly suitable for larger particles (>1000 μm) [*Van Rijn*, 1984a]. Therefore, the coefficient of proportionality in equation (33) needs to be calibrated for small particles. In the current submodel, the pickup rate formula proposed by *Nakagawa and Tsujimoto* [1980] is used for this calibration. This formula was validated against a range of physical observations. Moreover, the method of *Nakagawa and Tsujimoto* [1980] yielded one of the best predictions of the pickup function for fine sediment, as reported by *Van Rijn* [1984a]. This approach was also effectively used by *Onda and Hosoda* [2004], *Giri and Shimizu* [2006], and *Shimizu et al*. [2009] in models of bedform development. *Nakagawa and Tsujimoto* [1980] express the dimensionless pickup rate by

$$P^*_S = \frac{P_S\sqrt{d}}{\sqrt{\left(\rho_p/\rho - 1\right)g}} = F_0\overline{\tau}^*\left(1 - \frac{\overline{\tau}^*_{cr}}{\overline{\tau}^*}\right)^3 \tag{38}$$

in which F_0 is an experimental constant. The variables $\overline{\tau}^*$ and $\overline{\tau}^*_{cr}$ are the dimensionless shear stress and the critical shear stress for incipient motion, respectively, both averaged over time and space. According to the experimental studies of *Nakagawa and Tsujimoto* [1980], suitable values for the constants in equation (38) are $F_0 = 0.03$ and $\overline{\tau}^*_{cr} = 0.035$. The factor P_S can be considered as the probability density of sand particle dislodgment per unit time from the bed area occupied by one sediment particle [*Nakagawa and Tsujimoto*, 1980].

[44] Equation (38) is based on unidirectional flow over a flat bed. *Nagata et al*. [2005] used Tsujimoto's pickup rate formula to find the volumetric rate of sediment pickup from a specific area on the bed. Applying this approach to a cellcovering part of the bed yields

$$\dot{\overline{V}}_S = \frac{A_3}{A_2}P_S S d \tag{39}$$

[45] Here $\dot{\overline{V}}_S$ is the volume of sediment pickup per unit time, S is the area of the cell on the bed-surface, and A_2 and A_3 are shape coefficients for spherical sand grains with two- and three-dimensional geometrical properties, namely $\pi/4$ and $\pi/6$ respectively.

[46] In order to validate and calibrate the erosion rate in equation (33), flow computations are made for different discharges over a flat bed, yielding different bed shear stress levels. The computed results are averaged over time and space to find the average entrainment rate and the average shear stress. The instantaneous volumetric pickup rate over area S can be written as

$$\dot{V}_E = E\frac{S}{\rho_p} \tag{40}$$

[47] The computed average entrainment rates $\dot{\overline{V}}_E$ are compared with the entrainment rate according to equation (39). Figure 6 shows that the computed average entrainment (based on the mean shear stress) agrees well with that derived from equation (39). The best fit for factor ψ in equation (33) is found to be 3.67×10^{-4}.

[48] The volume of sediment pickup in a time interval Δt will be

$$V_E = \dot{V}_E\Delta t = E\frac{S}{\rho_p}\Delta t \tag{41}$$

[49] The number of particles involved can be determined by dividing the pickup volume by the volume of a single particle V_p.

$$n_{pickup} = \frac{V_E}{V_p} \tag{42}$$

[50] The number of particles picked up may be large, so that treating them one by one is beyond the capacity of existing computational resources. Hence we use a multiplication factor, usually smaller than 1 (for fine sediment), to decrease the number of particles for computational efficiency. In this way, we consider a smaller number of particles, but with the same total volume of pickup: we assume each particle to carry the mass of a number of its neighbors. The mass carried by a particle can be calculated as

$$m'_p = \frac{m_p}{C_{frac}} \tag{43}$$

where m_p is the mass of a physical particle, m'_p is the mass carried by the computational particle, and C_{frac} is the multiplication factor. After the particle has been lifted, it may be transported by the flow. The next section describes the equations of motion of particles in flow.

4.2. Sediment Transport in the Water Column

[51] After pickup, the particles are transported by the forces exerted by the flow. According to *Maxey and Riley*

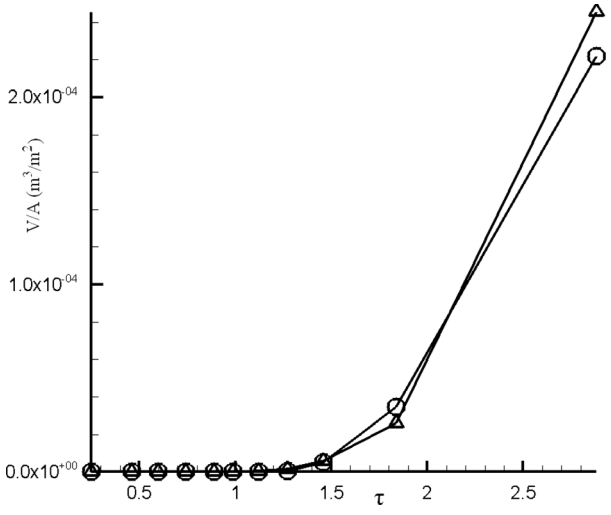

Figure 6. Comparison between the averaged computed entrainment and the entrainment rate from the relation of *Nakagawa and Tsujimoto* [1980].

[1983], the velocity of an individual sediment particle in the flow is described by

$$\rho_p V_p \frac{\mathrm{d}\vec{v}_p}{\mathrm{d}t} = \left(\rho_p - \rho\right) V_p \vec{g} + \rho V_p \frac{D\vec{u}_f}{Dt} + \frac{1}{2}\rho V_p \left(\frac{D\vec{u}_f}{Dt} - \frac{\mathrm{d}\vec{v}_p}{\mathrm{d}t}\right) + \frac{3}{4}\frac{C_D}{d}\rho V_p |\vec{u}_f - \vec{v}_p|\left(\vec{u}_f - \vec{v}_p\right) + \frac{3}{4}\frac{C_L}{d}\rho V_p \left(|\vec{u}_f - \vec{v}_p|^2_{top} - |\vec{u}_f - \vec{v}_p|^2_{bottom}\right)\vec{n} \tag{44}$$

where $\vec{u}_f$ represents the fluid velocity at the particle location, $\vec{v}_p$ is the velocity of the sediment particle, d is the particle diameter, C_L is the lift coefficient, C_D is the drag coefficient, $D/Dt = \frac{\partial}{\partial t} + \vec{u}.\nabla$, V_p is the particle volume, $\vec{g}$ is the gravity vector, and ρ and ρ_p are the densities of the fluid and particle, respectively. The first term in the right-hand side of equation (44) represents the gravity force. The second and third terms are the effect of pressure and added mass, respectively [*Maxey and Riley*, 1983]. The drag coefficient C_D can be found from equation (2), but the lift coefficient C_L is difficult to determine. There is limited knowledge regarding the effect of solid boundaries on the particles. The effect of shear stress has been studied for very simple linear cases with $Re_p \ll 1$. Moreover, the fluid velocity needs to be determined at the top and the bottom of the particle. In the model, the size of a particle is 1 or 2 orders of magnitude smaller than the size of a computational grid cell, which makes the difference between the interpolated velocities at the top and the bottom of a particle insignificant. We therefore replace the lift force term in equation (44) by the theoretical and experimental relations introduced by *McLaughlin* [1991] and *Mei* [1992], which are given in equations (4) and (6). These equations parameterize the total lift force, including Magnus effect and wall drift force.

[52] A major simplification in the present study is that we neglect the interactions between the suspended particles as well as the effect of particles on the fluid flow. This simplification is valid if the sediment concentration in the mixture of water and sediment is low.

[53] Equation (44) is solved numerically using an implicit scheme to avoid instabilities. The position of each particle is then determined as

$$\frac{\mathrm{d}\vec{x}_p}{\mathrm{d}t} = \vec{v}_p \tag{45}$$

where $\vec{x}_p$ is the position vector of the particle. The particles move according to equations (44) and (45), until they settle. The mechanism of deposition is discussed in the next section.

[54] The simulation of sediment transport is the most time-consuming part in the current sediment model as the number of suspended particles can be large. Hence, the sediment transport is parallelized by OpenMP on shared memory computers. It is the novelty of the model that with a simple parallelization, without message passing interface (MPI), by using multicore personal computers, it can still handle the calculations of large eddy simulation with particle motions in a relatively time-efficient way. This is realized by the combination of an efficient hydrodynamic model and an efficient sediment motion model.

4.3. Sediment Deposition

[55] Previous studies give conflicting assessments as to whether depositing grains rebound partially elastically or are viscously damped [*Schmeeckle et al.*, 2001]. All researchers who modeled the collision of saltating grains in water use the same simple model: the incoming velocity of the impacting grain is divided into two components; normal and tangential to the colliding surface. The outgoing tangential velocity is equal to the incoming tangential velocity times a coefficient α_t, and the outgoing normal velocity is equal to the incoming normal velocity multiplied by a factor α_n.

[56] What happens exactly when depositing particles hit the bed is not clearly known yet. Particles can interact with the bed in different ways. Their motion may be viscously damped, they may be reflected or they may move tangentially to the bed. *Schmeeckle et al.* [2001] showed that appropriate physical scaling of this problem requires similitude of a collision Stokes number:

$$St = \frac{m_p v_p}{6\pi\mu r_*^2} \tag{46}$$

where m_p is the mass of a single particle, μ is the dynamic viscosity of the water, v_p is the particle velocity when it hits the bed, and r^* is the relative particle radius $\left(1/r^* = 1/r_p + 1/r_{st}\right)$. The variables r_p and r_{st} are the radii of the moving particle and the stationary particles located on the bed, respectively. The Stokes number (St) is a measure of the inertia of the particle relative to the viscous pressure force exerted on it by the fluid. Hence, if $St \ll 1$, the viscous pressure stops the particle before significant elastic energy can be stored in the deformation of the particles. In this case, there will be no initial rebound velocity. At moderate values of St, the elastic deformation becomes significant enough to develop an initial rebound velocity but the rebounding particle will be arrested by negative pressure and cavitation in the gap between it and the bed. At still higher values $(St \gg 1)$, rebounding particles separate completely.

[57] Figure 7, from an experimental study by *Schmeeckle et al.* [2001], shows a graph of the transition from viscously damped to partially elastic collisions. According to this figure, the transition between damped and undamped particle collisions occurs at about the transition from medium to coarse sand. The corresponding critical sediment diameter size is 2.7 mm. Therefore, for sediment larger than sand (>2 mm), saltation impacts are almost always partially elastic, whereas no significant normal rebound occurs for sand and smaller particles.

[58] According to this information, for bed-load transport of sand (<2 mm), the normal elastic coefficient α_n is zero, because the collisions are viscously damped. The tangential elastic coefficient α_t takes a value of about 0.9 [*Schmeeckle et al.*, 2001]. For particles larger than sand, the critical Stokes number ranges between 39 and 105. At Stokes numbers higher than 105, partially elastic collisions occur, and the new velocities can be calculated as follows

$$v_{n,new} = -\alpha_n v_{n,old} \tag{47}$$

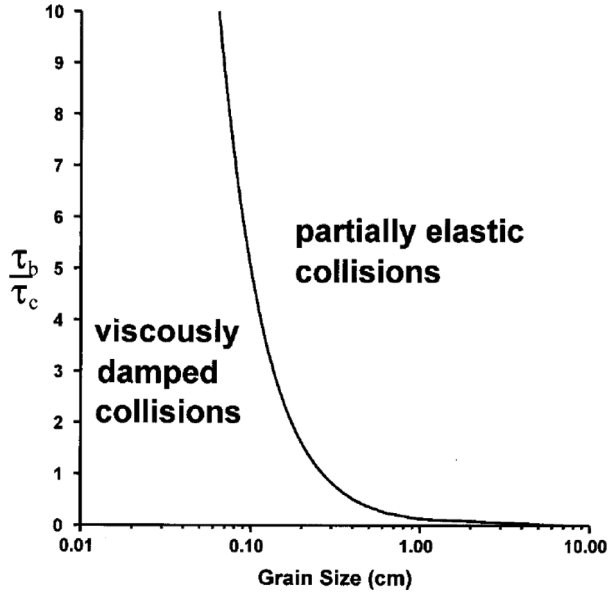

Figure 7. Graph of the transition from viscously damping to partially elastic collisions at typical bed load saltation velocities as a function of grain size and transport stage τ_b/τ_c, where τ_b is the boundary shear stress and τ_c is the Shields critical shear stress. Taken from *Schmeeckle et al.* [2001].

$$v_{t,new} = \alpha_t v_{t,old} \tag{48}$$

[59] Here, v_n and v_t are the normal and tangential velocities of the particle during deposition, respectively. *Schmeeckle et al.* [2001] experimentally determined α_n at a value of 0.65. For Stokes numbers less than 39, the particle motion is viscously damped. In the range between 39 and 105, the behavior is not clear because of the negative pressure and cavitation between the particle and the bed. *Schmeeckle and Nelson* [2003] applied equations (47) and (48) for Stokes number less than 105, but set the normal rebound coefficient at zero $(\alpha_n = 0)$. This approach is also taken in the present submodel for sediment deposition.

4.4. Sediment Transport Over the Bed

[60] If the angle, φ, calculated from equation (25) does not fall within the range of $\pi/3 \leq \varphi \leq 2\pi/3$, the particle cannot separate and will roll or slide along the bed. This can also be observed in flume experiments and in the field: a significant fraction of sediment transport occurs in this way. An extreme manifestation of this phenomenon is fluidization of the bed under high shear stresses.

[61] This kind of sediment transport cannot be modeled in the same way as the transport of particles in the fluid described in section 4.2. Therefore, we need another submodel, describing sediment transport in layers over the upper part of the bed. Here we develop a simple bed-load submodel, considering the bed load as a sheet moving from one computational cell to the other. Figure 8 shows this submodel schematically for one cell on the bed. The sediment sheet can only move in the direction of the exerted force. Assuming the force, exerted on the particle, to be constant over a time step Δt, it yields

$$a_t = \frac{F_t}{m_p} \tag{49}$$

where a_t is the acceleration due to force F_t and m_p is the mass of a solitary particle. We suppose that the motion of each solitary particle starts from rotation as shown in Figure 4. If F_t exceeds the critical level, but is not sufficient to separate the particle from the bed, the particle will roll or slide after it reaches point P in Figure 4. This point corresponds with angle $\pi/2$. The initial angular velocity can be determined according to equation (23). The center of rotation of the particle is the center of particle 2 located in the bed. Thus, the tangential velocity $v_{0,tan}$ can be determined as

$$v_{0,tan} = \mathrm{d}\omega \tag{50}$$

where ω is the radial velocity of the center of the moving particle.

[62] We suppose that the time necessary to rotate the particle to the summit of the supporting particle (point P) is negligible. Thus, the displacement δ can be calculated as follows

$$\delta = 0.5 a_t \Delta t^2 + v_{0,tan} \Delta t \tag{51}$$

[63] It can be projected in x and z directions

$$\delta x = \delta . t_x \tag{52}$$

$$\delta z = \delta . t_z \tag{53}$$

where t_x and t_z are the components of the tangential unit vector $\vec{t}$ (in the direction of $\vec{F}_t$), respectively.

[64] The amount of sediment pickup is calculated by equation (33). After displacement of the sediment layer, the amount of sediment given to a neighboring cell can be determined as the ratio of the area displaced to the neighbor cell to the total area multiplied by the amount of sediment

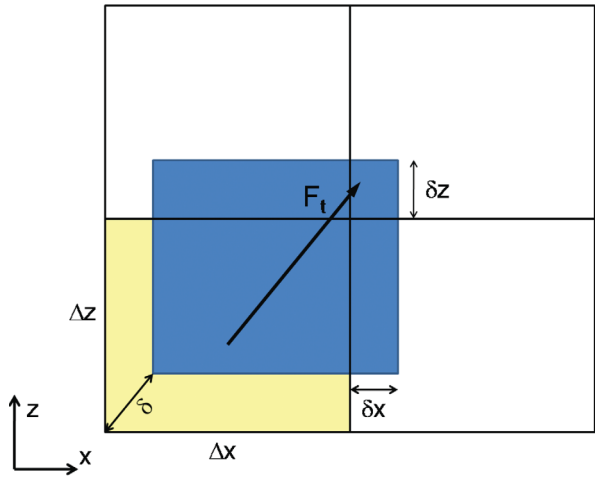

Figure 8. Model for rolling and sliding of sediment after pickup if sediment particles cannot leave the bed. A layer of sediment on the cell moves in the direction of the tangential force and slides to the neighbor cells.

picked up. For example, the sediment passed on to the eastern cell in Figure 8 can be determined by

$$P_{S,east} = \frac{\delta x(\Delta z - \delta z)}{\Delta x \Delta z} P_S \tag{54}$$

[65] This submodel describes the part of the bed-load transport without saltation. The combination with the submodel for transport of saltating and suspended particles in the water column provides the total sediment motion on and above the bed.

5. Numerical Implementation

5.1. Pickup

[66] Three major forces are considered for the sediment particles during pickup: drag force, lift force, and gravity. The drag, lift, and gravity forces are calculated by equations (1), (5), and (7), respectively. The flow velocity at the particle level which is required for the drag and lift is interpolated in a way similar to the ghost-cell technique in *Nabi et al*. [2012]. The normal vector of the bed at the sediment level is extended to form an imaginary point. The flow is interpolated trilinearly for the imaginary point, and the flow velocity at the particle level is interpolated by a log-law function from the imaginary point.

[67] As the forces are calculated, they are projected to tangential and normal directions using equations (11) and (12), and the moment acting on a particle is calculated. In the case of a positive moment, the particle rotates. The angle of separation and the initial velocities are calculated by equations (25) and (26), respectively. If the angle of separation falls in the required range ($\pi/3 \leq \varphi \leq 2\pi/3$), the particle separates and goes into the flow, for which the submodel for transport in the water column governs its subsequent motion. If the separation angle is not in the required range, the submodel for transport over the bed shifts a layer of sediment on the cell area to the neighboring cells in the direction of the flow. The volume of the sediment pickup and hence the number of particles picked up is determined by equations (41) and (42). As the forces are considered to be uniform within each cell area on the bed, the particles are distributed randomly in the cells to avoid following a unique path.

5.2. Transport in the Water Column

[68] In the case of separation of particles from the bed in the pickup stage, the flow acts on the particle in a transport mode. Equations (44) and (45) are applied for the particle velocities and trajectories, respectively. The drag, lift, and gravity are calculated with the similar procedure as for the pickup phase, except that the flow velocities are interpolated by a sixth-order Lagrangian interpolation. The locations of the particles are monitored in each time step, and if a particle comes into contact with the bed, the deposition submodel starts.

5.3. Transport Over the Bed

[69] Transport over the bed occurs if the forces on the sediment particles do not allow separation from the bed. A sheet of sediment moves in the direction of the flow from the cell to its neighbors. The volume of sediment (the thickness of the sheet) is calculated by equation (41) for pickup.

5.4. Deposition

[70] In case a particle comes into contact with the bed, as mentioned above, it may either be damped viscously or rebound and return into the water column. In the case of rebounding, the normal vector at the contact point is calculated, and the normal and the tangential velocities are found. The tangential velocity is kept constant, and the normal velocity is multiplied by a negative value smaller than unity (elasticity factor). If the condition does not satisfy the rebounding process, the particle is added to the deposited-particles number for the cell where the particle comes into contact with the bed. This number identifies the volume of sediment deposition in that cell. After this calculation, the volume is used to deform the bed, which is discussed in the companion paper on the development of ripples and dunes (M. Nabi et al., submitted manuscript, 2013).

6. Numerical Validation

6.1. Particle Settling Velocity

[71] Basically, the settling velocity is not a particle property, but rather a behavioral property. The terminal settling velocity (w_s) of a particle occurs when the fluid drag force on the particle is in equilibrium with the gravity force. Considering equations (1) and (7) for the drag and gravity forces, the fall velocity takes the following form [*Swamee and Ojha*, 1991].

$$w_s = \sqrt{\frac{4}{3}\frac{\left(\rho_p/\rho - 1\right)dg}{C_D}} \tag{55}$$

[72] In order to show how this constant velocity is reached, a particle of 0.25 mm diameter is released in the numerical model from a stationary state in a steady flow. Figure 9a shows the computed time evolution of the settling velocity and the drag coefficient. The velocity increases and approaches a constant value. The drag coefficient decreases and also approaches a constant value. In equation (55), the drag coefficient C_D is a function of the settling velocity w_s, making this relationship implicit. It can be solved iteratively to determine the values of the mentioned variables. Figure 9b shows the result for the same sediment diameter. Figure 9 clearly shows that the numerical results agree well with the analytical solution.

6.2. Sediment Avalanching

[73] During the formation of dunes, the angle of the lee side may become relatively steep. If this angle is larger than the angle of repose, it is possible that the sediment slides along the lee side to the bottom. This process is called avalanching. Avalanching occurs because of instability of the sediment pack caused by gravity. If the direction of the gravity force falls outside the stability region of the particles, it tends to pull the particles downward. If opposing hydraulic forces are absent or not strong enough, avalanching occurs. It has to be noticed that in the current model, the avalanching is based on the motion of solitary particles, and the effect of geometrical interactions between

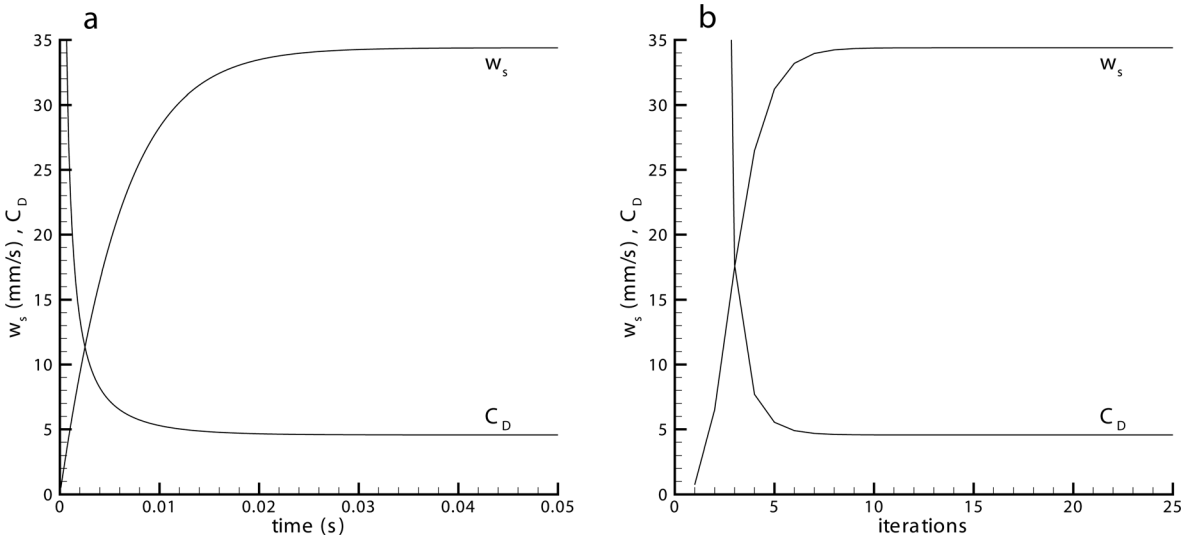

Figure 9. The fall velocity of a particle with diameter $d = 0.25$ mm by (a) simulation and (b) iteration of equation (55).

particles, which leads to pack avalanching, is not taken into account. This model is hence suitable for noncohesive uniform sediment, as the avalanching occurs in the form of small bulks.

[74] In the present model, avalanching occurs automatically (by balance of forces), and no extra restrictions are applied. Yet, as grain-grain interactions within the bed are not considered, this model is tested for its capability to reproduce the empirical values of the angle of repose. As a test case, we start from a steep sediment mound of 75° under stagnant water. The initial slope of 75° is much larger than the angle of repose. Figure 10 shows the initial condition of the bed. Although there is no ambient flow, the mound collapses. The particles move downhill, the height of the mound decreases, and the width at the toe increases. Figure 11 shows the avalanching as a function of time. The slope of the deformed bed decreases until it reaches the angle of repose. Then the downhill transport of sediment stops and the bed reaches a steady state. Our model results in an angle of repose of 30°, as can be concluded from Figure 11. Experimental measurements give an angle of repose between 26 and 34° for sands [*Chanson*, 2004].

6.3. Bed Load Sediment Transport

[75] The aim of this section is to compare the sediment transport rate resulting from the present model with empirical relations from previous studies. Since more than a century, researchers have been developing methods to calculate the bulk bed-load flux. One of the simplest bed-load transport formulae was developed by *Meyer-Peter and Müller* [1948]. They conducted experiments for a sediment bed with varying grain size ($d = 0.03 - 2.9\text{cm}$) and with different sediment densities ($\rho_s = 1.3 - 4.2\text{g/cm}^3$). Their empirical relation for the bed load flux at high shear stress is

$$q_b^* = 8\left(\tau^* - \tau_{cr}^*\right)^{3/2} \tag{56}$$

[76] Equation (56) represents a general bed-load formula, where $\tau_{cr}^* = 0.047$ is an average value of nondimensional critical shear stress, τ^* is the nondimensional shear stress, and q_b^* is the nondimensional bed-load transport rate, defined as

$$q_b^* = \frac{q_b}{d\sqrt{\left(\rho_p/\rho - 1\right)gd}} \tag{57}$$

[77] However, research in the past two decades has shown that the constant 8 and even the exponent 3/2 needs to be reassessed for nonsmooth beds. Different values were obtained for example by *Hunziker* [1995] or *Wong and Parker* [2006] for rippled beds. These differences are discussed by *Tritthart et al.* [2011]. If we simulate sediment transport over a smooth bed, the bed-load transport formula by *Meyer-Peter and Müller* [1948] gives proper results.

[78] *Wiberg and Smith* [1987] pointed out that the observed variation in the transport coefficient is well captured by a simple dependence on the Shields stress (τ^*), yielding a generalized bed-load transport relation:

$$q_b^* = \alpha\left(\tau^* - \tau_{cr}^*\right)^n \tag{58}$$

where $n = 3/2$ and

$$\alpha = 1.6\ln(\tau_*) + 9.8 \approx 9.64\tau_*^{0.166} \tag{59}$$

[79] Einstein and others used a different approach to estimate the sediment transport rates. This approach takes into account the effect of the fluctuating flow field on the probability of the entrainment of particles within a population [*Einstein*, 1942; *Brown*, 1950], and it also considers the armoring effects and the intensity of turbulent fluctuations near the bed. Under equilibrium conditions the number of grains deposited must be equal to the number of grains eroded, which, along with experimental data fitting, gives

$$q_b^* = 40K\tau_*^3 \tag{60}$$

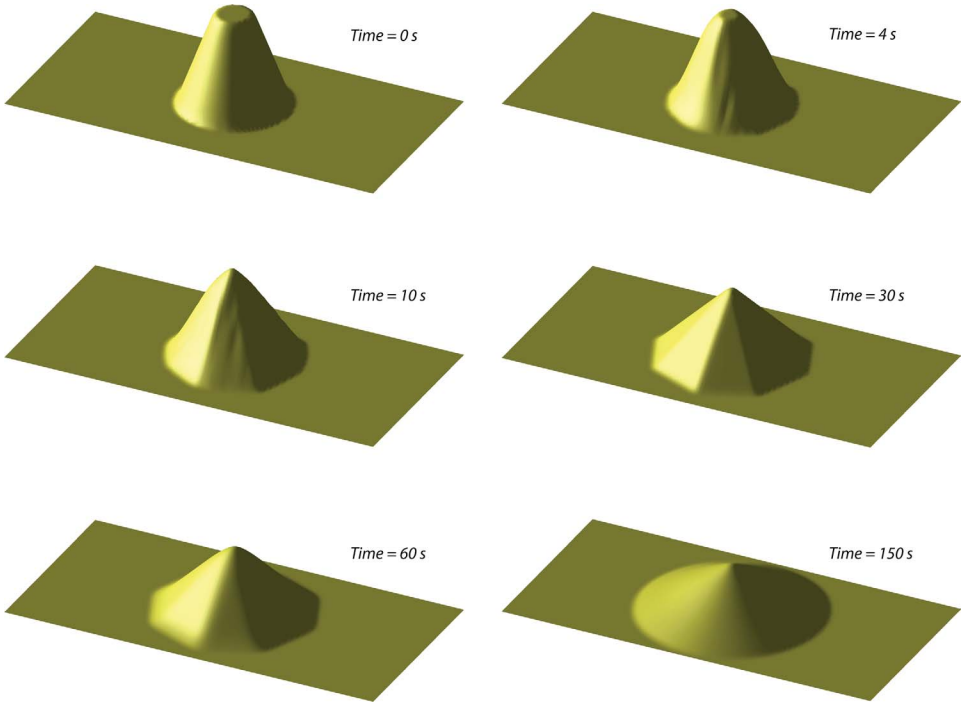

Figure 10. Three-dimensional views of the computed avalanche. It begins from a steep angle and the angle decreases until it reaches the angle of repose.

where

$$K = \sqrt{\frac{2}{3} + \frac{36\nu^2}{\left(\rho_p/\rho - 1\right)gd^3}} - \sqrt{\frac{36\nu^2}{\left(\rho_p/\rho - 1\right)gd^3}} \tag{61}$$

[80] *Van Rijn* [1984b] proposed a different formula which can be used to estimate bed-load transport rates with mean sediment sizes in the range between 0.2 and 2 mm. This formula is given as

$$q_b^* = 0.053 \frac{T^{2.1}}{d_*^{0.3}} \tag{62}$$

where d^* and T are the dimensionless mean particle diameter and transport stage parameter, respectively, and defined as

$$d^* = d\left[\frac{g\left(\rho_p/\rho - 1\right)}{\nu^2}\right]^{1/3} \tag{63}$$

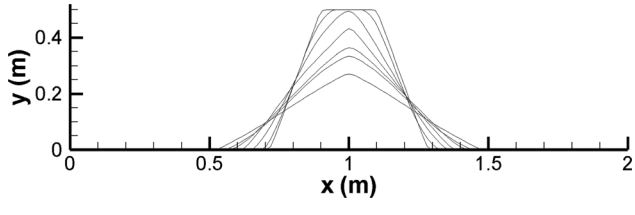

Figure 11. Cross sections of the bed during avalanching.

$$T = \frac{\overline{\tau}^* - \overline{\tau}_{cr}^*}{\overline{\tau}_{cr}^*} \tag{64}$$

[81] Here $\overline{\tau}_{cr}^*$ is the critical shear stress from the Shields diagram.

[82] In our numerical model, the sediments are transported as single particles in a Lagrangian framework. To estimate the bed-load transport rate (or the total load transport rate), the total number of sediment particles passing through a plane normal to the streamwise direction is counted. As the model moves the particles at each time step Δt, the passing volume is the volume of sediment which passes the intersection in a time interval Δt over the width of the channel. Dividing the volume by Δt and the width, it gives the volumetric transport rate per unit width:

$$q = \frac{n_{pass} V_p}{b\Delta t} \tag{65}$$

in which n_{pass} is the number of passing sediment particles, b is the width of the channel, and q is the total load transport rate yielding from the numerical model.

[83] The sediment transport is simulated for several flow rates and grain sizes (yielding different values of the Shields stress). Figure 12 shows a comparison of the sediment transport rates from the present model with Meyer-Peter and Müller's, Wiberg and Smith's, van Rijn's, and Einstein's formulae. It is important to note, however, that the simulations were done with a completely flat bed and that we used the zero velocity level as a calibration factor to tune the transport rate. The zero velocity level is found to be 0.25 d under the top of the particles on the bed, which agrees well with *Van Rijn* [1984b]. Figure 12 shows that the simulation results agree well with Meyer-Peter and

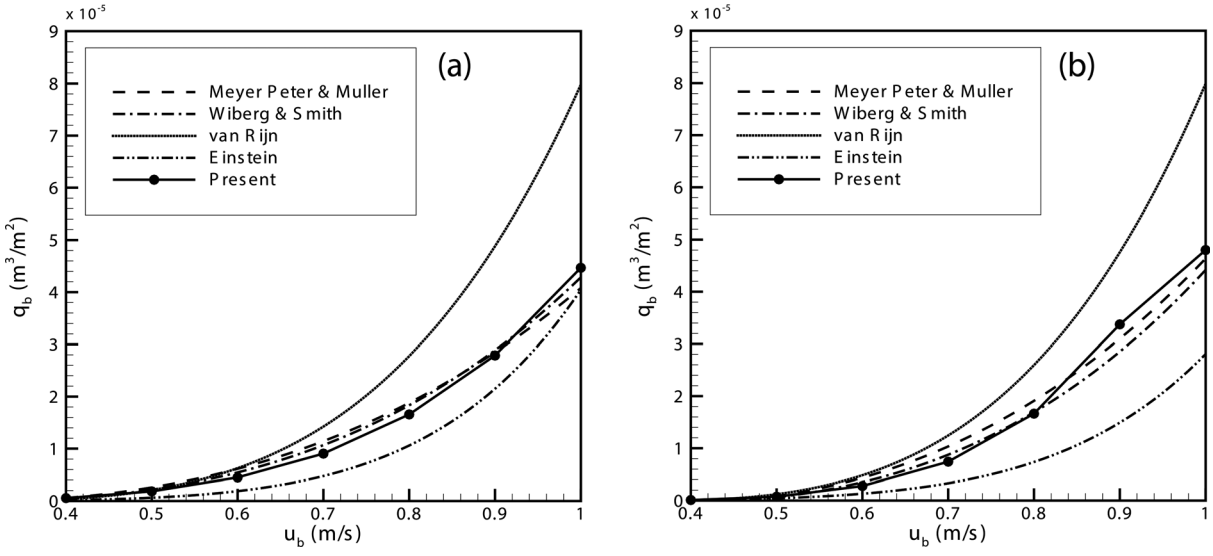

Figure 12. Sediment transport computed by the present model and compared with some parameterized relations for different grain sizes with (a) 300 μm and (b) 650 μm.

Müller's and Wiberg and Smith's formulae and have the same order of magnitude as the predictions from the other empirical relations.

6.4. Sediment Concentration in a Straight Channel

[84] By considering sediment with a constant settling velocity in uniform stationary flow, the suspended sediment concentration in the vertical direction satisfies the Rouse distribution [*Rouse*, 1937]. This theoretical distribution can be applied in situations where sediment concentration c_a at one particular elevation above the bed $z = a$ can be quantified. It is given by the expression:

$$\overline{c} = c_a \left(\frac{h - z}{z} \frac{a}{h - a} \right)^{\frac{w_s}{\kappa u_*}} \tag{66}$$

where u_* is shear velocity, z is the distance from the bed, κ is von Kármán's constant, with a value of approximately 0.4, and h is the water depth. The Rouse profile is valid for nonhyperconcentrated water-sediment mixtures. The Rouse parameter (the exponent in equation (66)) denotes the ratio of the downward settling velocity to the shear velocity representing the upward velocities caused by turbulent fluctuations. The settling velocity can be found from equation (55), and the shear velocity u_* can be found as [*Van Rijn*, 1993]

$$u_* = \frac{\kappa u_b}{\left[\ln\left(\frac{h}{z_0}\right) + \frac{z_0}{h} - 1 \right]} \tag{67}$$

where u_b is the bulk velocity and z_0 is the level of zero intercept near the bed. The value of z_0 is related to the effective roughness height k_s and defined as $z_0 = k_s/30$ with $k_s = 2.5d$. The bulk velocity follows directly from the flow discharge via $u_b = Q/A$, where A is the cross-sectional area.

[85] In order to validate the sediment transport submodel, suspended sediment in a straight channel with uniform flow is simulated and the vertical sediment concentration profile is compared with the Rouse distribution. After the particles have reached statistically steady motion, the number of particles is determined in thin layers parallel to the bed and the total volume of particles is divided by the total volume of the layer. Figure 13 compares the concentration profile thus obtained with the theoretical Rouse distribution for a grain size of 150 μm and a bulk velocity of 0.9 m/s. The simulated concentration profile is found to be in a good agreement with the theoretical profile.

6.5. Sediment Saltation

[86] A number of numerical tests are conducted to assess the capacity of the proposed particles-based numerical model to simulate the saltation mechanism under steady

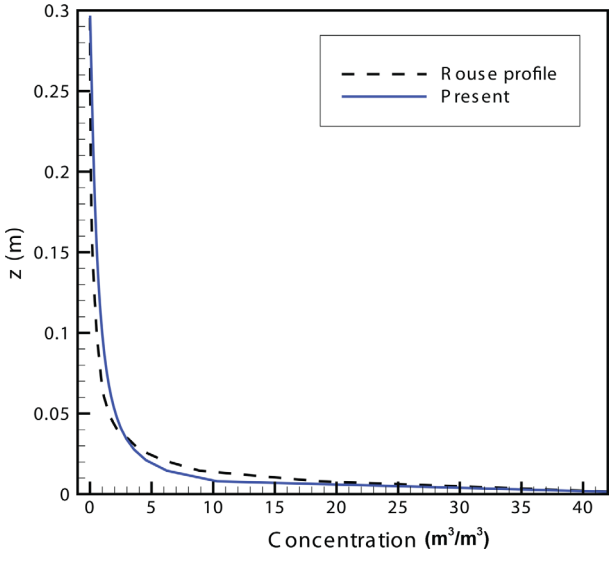

Figure 13. Comparison between theoretical and simulated Rouse profiles for sediments with diameter 150 μm and a bulk velocity of 0.9 m/s.

Table 1. Experimental Conditions of *Niño and García* [1998]

Experiment	h (m)	u_* (m/s)	h/d_p	Fr	Re
S11	0.0285	0.0207	53.8	0.515	7750
S12	0.0347	0.0240	65.5	0.541	10955
S13	0.0398	0.0266	75.1	0.561	13941
S14	0.0430	0.0282	81.1	0.572	15971
S15	0.0463	0.0299	87.4	0.583	18188
S16	0.0509	0.0321	96.0	0.598	21484

discharge conditions. The results are compared with a series of experiments conducted by *Niño and García* [1998] in a rectangular flume with a length of 18.6 m, a width of 0.297 m, and a slope of 0.0009.

[87] The flume bed was fixed and composed of uniform sand particles (diameter of 0.53 mm). The flow depth in the experiments ranged between 28 and 50 mm. The Reynolds number of the flow varied from about 7800 to about 21,500. The flow was subcritical, and the values of the Froude number were in the range from about 0.5 to about 0.6. Table 1 shows the experimental conditions.

[88] Here we simulated the experiments using the present sediment motion model. The numerical conditions are identical to the experimental conditions of Table 1, except for the flume length and width. A square part of flume, with a length and width of 0.114 m, is considered. To avoid sidewall effects, the boundaries in streamwise and transverse directions are set to periodic. A flat bed with a uniform sediment size of 0.53 mm is considered. In order to generate significant turbulence structures an initial perturbation is given to the bed. The presence of irregularities on the bed has a major role in maintaining the successive saltation process [*Sekine and Kikkawa*, 1992]. The imposed heights of the bed perturbations are in the order of the grain size.

[89] The sediment transport is turned on after the flow has reached its statistically homogenous steady state. Subsequently, the locations of the pickup, deposition, and the maximum height from the bed are stored and averaged in time and space. Moreover, the time between pickup and deposition is also stored and averaged. Knowing the duration of the saltation event, T_s, the associated mean streamwise particle velocity U_s is obtained as

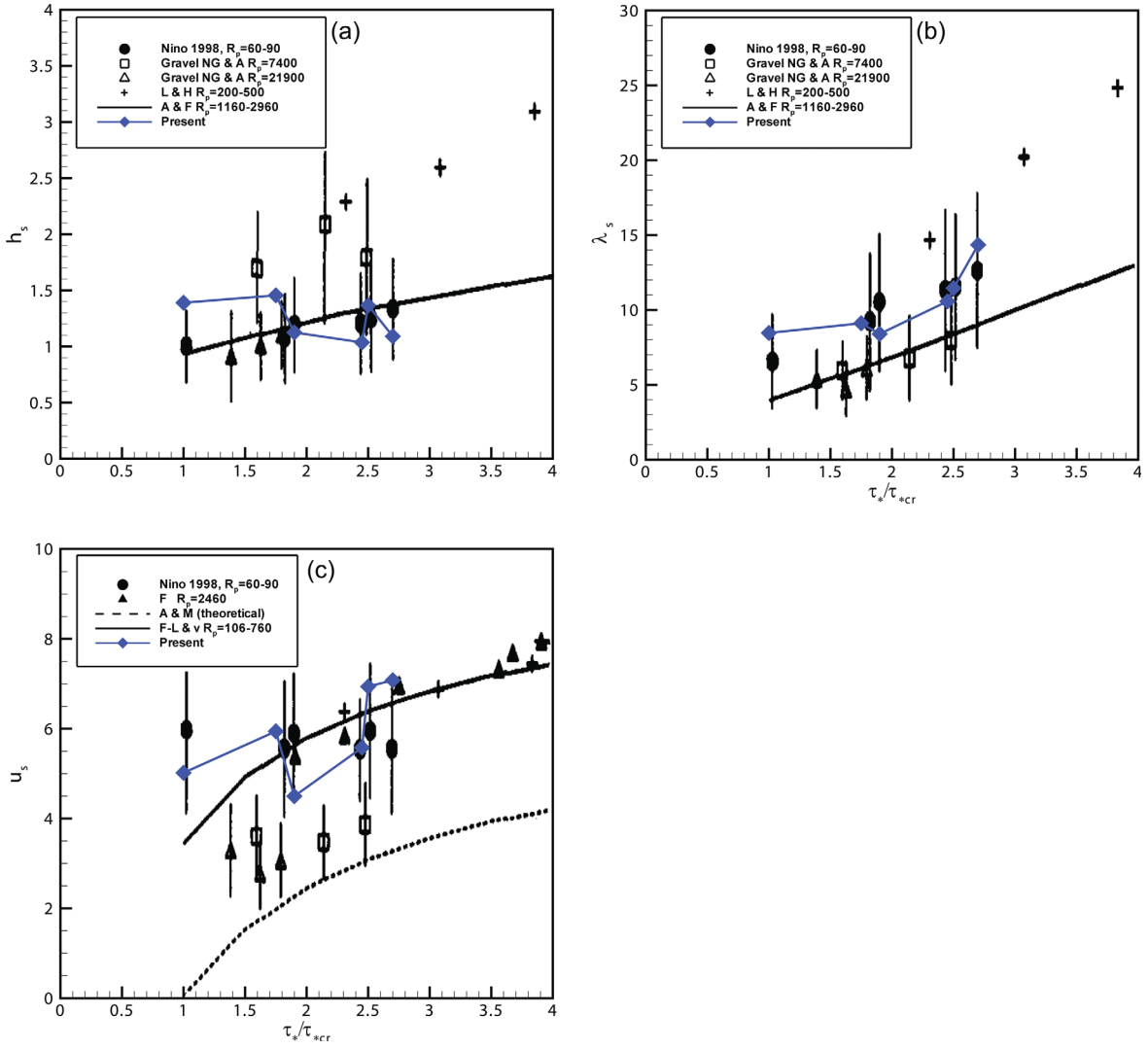

Figure 14. Comparison between experimental and simulated (a) saltation length, (b) saltation height, and (c) saltation velocity.

$$U_s = \frac{L_s}{T_s} \tag{68}$$

where L_s denotes the saltation length. Then, we determined ensemble averages of saltation height, length, and streamwise particle velocity, which are made dimensionless in the form of $h_s = H_s/d$, $\lambda_s = L_s/d$, and $u_s = U_s/u_*$; where H_s is saltation height with respect to the top of the bed grains. The dimensionless saltation length and height, obtained from the computational results, are plotted in Figures 14a and 14b as a function of τ^*/τ^*_{cr} together with those obtained by *Niño and García* [1998], *Niño et al*. [1994], *Abbott and Francis* [1977], and *Lee and Hsu* [1994]. Similarly, results for the dimensionless streamwise saltation velocity, obtained from the present numerical results, are plotted in Figure 14c as a function of the ration τ^*/τ^*_{cr}, together with those corresponding to gravel saltation [*Niño et al*., 1994]; the experimental results of *Francis* [1973], *Fernandez-Luque and van Beek* [1976], and *Lee and Hsu* [1994]; and the theoretical relation of *Ashida and Michiue* [1972].

[90] The saltation height from our computational results agrees well with the experimental measurements. However an overprediction for the low values of τ^*/τ^*_{cr} can be observed in Figure 14a. This is probably caused by a difference between the bed topography in the experimental setup and in our calculations, as the turbulence structures can be strongly affected by the initial bed perturbations. A similar behavior can be observed in Figure 14b for the low values of τ^*/τ^*_{cr}. However, our computational results fall inside the range of standard deviation of the experimental measurements, as they are in good agreement with the results of *Niño and García* [1998].

7. Conclusions

[91] We have developed a model for the simulation of sediment motion in turbulent flow. The sediment is considered to consist of uniform sand-size spherical particles, and its motion is modeled in a Lagrangian framework, which allows involving new concepts that are better suited for relatively small spatial and temporal scales. This approach gives a better insight into the physical transport phenomena and makes it possible to simulate details of the sediment motion, such as jumping, sliding, and rolling.

[92] The motion of sediment generally consists of three stages: (1) the particles begin to move (pickup), (2) they get transported (moving in the water column or rolling or sliding over the bed), and (3) they are deposited at other locations. These stages are all governed by gravitational and flow-induced forces, which are simulated using theoretical and empirical relations.

[93] The model has been validated for various well-documented aspects, such as the settling velocity of a single particle in stagnant water, the angle of repose after avalanching, the bulk flux and the concentration profile in uniform flow, and the saltation characteristics. In all cases, the model results agree well with known formulae and relations. This model is to be used in high-resolution morphodynamic simulations. This means that the present process-oriented validation is necessary, but not sufficient. Nabi et al. (submitted manuscript, 2013) combine the present submodels for sediment pickup, transport, and deposition with a model for evolution of the river bed. They validate the combined system against experimental data on the formation and migration of ripples and dunes.

[94] **Acknowledgments.** The work presented herein was carried out as part of the work package "River Morphology" of Delft Cluster project 4.30 "Safety against flooding," financed by the Netherlands government and supported by Rijkswaterstaat Waterdienst. The authors are grateful to Sanjay Giri for his fruitful suggestions.

References

Abbott, J. E., and J. R. D. Francis (1977), Saltation and suspension trajectories of solid grains in a water stream, *Philos. Trans. R. Soc. London A*, *284*, 225–254.

Allen, J. R. L. (1982), Sedimentary structures, their character and physical basis, in *Developments in Sedimentology*, vol. *30*(A,B), Elsevier, New York. Orientation of particles during sedimentation: Shape-Fabrics, in pp. 179–236

Armenio, V., and V. Fiorotto (2001), The importance of the forces acting on particles in turbulent flows, *Phys. Fluids*, *13*, 2437–2440.

Ashida, K., and M. Michiue (1972), Study on hydraulic resistance and bedload transport rate in alluvial streams, *Proc. Jpn. Soc. Civ. Eng.*, *206*, 59–69.

Auton, T. R. (1987), The lift force on a spherical body in a rotational flow, *J. Fluid Mech.*, *183*, 199–218.

Bridge, J. S. and J. L. Best (1998), Flow, sediment and bedform dynamics over the transition from dunes to upper-stage plane beds: Implications for the formation of planar laminae, *Sedimentology*, *35*, 753–763.

Brown, C. B. (1950), Sediment transportation, in *Engineering Hydraulics*, chap. 12, edited by H. Rouse, John Wiley, New York, N. Y.

Chanson, H. (2004), *The Hydraulics of Open Channel Flow: An Introduction*, 2nd ed., Elsevier. Oxford, UK, ISBN: 978 0 7506 5978 9.

Church, M. (2006), Bed material transport and the morphology of alluvial river channels, *Annu. Rev. Earth Planet. Sci.*, *34*, 325–354.

De Ruiter, J. C. C. (1982), The mechanism of sediment transport on bed forms, paper presented at Euromech Conference 156, Istanbul Tech. Univ., Istanbul, Turkey.

De Ruiter, J. C. C. (1983), Incipient motion and pick-up of sediment as function of local variables, *Tech. Rep. R657-XI*, Delft Hydraulics Lab., Delft, Netherlands.

Dey, S. (1999), Sediment threshold, *Appl. Math. Modell.*, *23*, 399–417.

Dey, S., and K. Debnath (2000), Influence of streamwise bed slope on sediment threshold under stream flow, *J. Irrig. Drain. Eng.*, *126*(4), 255–263.

Drew, D. A. (1978), The force on a small sphere in slow viscous flow, *J. Fluid Mech.*, *88*, 393–400.

Einstein, H. A. (1942), Formulae for transportation of bed-load, *Trans. ASCE*, *107*, 561–577.

Einstein, H. A., and E. A. El-Samni (1949), Hydrodynamic forces on rough wall, *Rev. Modern Phys.*, *21*(3), 520–524.

Escauriaza, C., and F. Sotiropoulos (2011), Lagrangian model of bed-load transport in turbulent junction flows, *J. Fluid Mech.*, *666*, 36–76.

Fernandez-Luque, R., and R. van Beek (1976), Erosion and transport of bed sediment, *J. Hydraul. Res.*, *14*(2), 127–144.

Francis, J. R. D. (1973), Experiments on the motion of solitary grains along the bed of a water stream, *Proc. R. Soc. London*, *332*(A), 443–471.

Giri, S., and Y. Shimizu (2006), Numerical computation of sand dune migration with free surface flow, *Water Resour. Res.*, *42*, W10422, doi:10.1029/2005WR004588.

Harper, E. Y., and I. D. Chang (1968), Maximum dissipation resulting from lift in a slow viscous shear flow, *J. Fluid Mech.*, *33*, 209–225.

Hunziker, R. P. (1995), Fraktionsweiser Geschiebetransport (Bedload transport in size fractions) [in German], *VAW Mitt.*, *138*.

Kurose, R., and S. Komori (1999), Drag and lift forces on a rotating sphere in a linear shear flow, *J. Fluid Mech.*, *384*, 183–206.

Lee, H., and I. Hsu (1994), Investigation of saltating particle motions, *J. Hydraul. Eng. ASCE*, *120*(7), 831–845.

Maxey, M. R., and J. J. Riley (1983), Equation of motion for a small rigid sphere in a nonuniform flow, *Phys. Fluids*, *26*(4), 883–889.

McEwan, I., and J. Heald (2001), Discrete particle modeling of entrainment from flat uniformly size sediment beds, *J. Hydraul. Eng.*, *127*(7), 588–597.

McLaughlin, J. B. (1991), Inertial migration of a small sphere in linear shear flows, *J. Fluid Mech.*, *224*, 261–274.

Mei, R. (1992), An approximate expression for the shear lift force on a spherical particle at finite Reynolds number, *Int. J. Multiphase Flow*, *18*(1), 145–147.

Meyer-Peter, E., and R. Müller (1948), Formulas for bed-load transport, paper presented at Proceedings of the 2nd Meeting of the International Association for Hydraulic Structures Research, Stockholm, Sweden.

Michaelides, E. E. (2006), *Particles, bubbles and drops: Their motion, heat and mass transfer*, World Scientific Publishing, Singapore.

Morsi, S. A., and A. J. Alexander (1972), An investigation of particle trajectories in two-phase flow systems, *J. Fluid Mech.*, *55*(2), 193–208.

Nabi, M., H. J. de Vriend, E. Mosselman, C. J. Sloff, and Y. Shimizu (2012), Detailed simulation of morphodynamics: 1. Hydrodynamic model, *Water Resour. Res.*, *48*, W12523, doi:10.1029/2012WR011911.

Nagata, N., T. Hosoda, T. Nakato, and Y. Muramoto (2005), Three-dimensional numerical model for flow and bed deformation around river hydraulic structures, *J. Hydraul. Eng., ASCE*, *131*(12), 1074–1087.

Nakagawa, H., and T. Tsujimoto (1980), Sand bed instability due to bed-load motion, *J. Hydraul. Div., ASCE*, *106*(12), 2029–2051.

Nelson, J. M., R. L. Shreve, S. R. McLean, and T. G. Drake (1995), Role of near-bed turbulence structure in bed load transport and bed form mechanics, *Water Resour. Res.*, *31*(8), 2071–2086.

Niño, Y., and M. García (1998), Experiments on saltation of sand in water, *J. Hydraul. Eng.*, *124*(10), 1014–1025.

Niño, Y., M., García, and L., Ayala (1994), Gravel saltation. 1. Experiment, *Water Resour. Res.*, *30*(6), 1907–1914.

Onda, S., and T. Hosoda (2004), Numerical simulation on development process of dunes and flow resistance, *Proc. River Flow*, *1*, 245–52.

Papanicolaou, A. N., P. Diplas, N. Evaggelopoulos, and S. Fotopoulos (2002), Stochastic incipient motion criterion for spheres under various bed packing conditions, *J. Hydraul. Eng.*, *128*(4), 369–380.

Rouse, H. (1937), Modern conceptions of the mechanics of fluid turbulence, *Trans. ASCE*, *102*, 463–543.

Rubinow, S. I., and J. B. Keller (1961), The transverse force on a spinning sphere moving in a viscous fluid, *J. Fluid Mech.*, *11*, 447–459.

Saffman, P. G. (1965), The lift on a small sphere in a slow shear flow, *J. Fluid Mech.*, *22*(2), 385–400.

Schmeeckle, M. W., J. M. Nelson, J. Pitlick, and J. P. Bennett (2001), Interparticle collision of natural sediment grains in water, *Water Resour. Res.*, *37*(9), 2377–2391.

Schmeeckle, M. W., and J. M. Nelson (2003), Direct numerical solution of bedload transport using local, dynamic boundary condition, *Sedimentology*, *50*, 279–301.

Shields, A. (1936), Anwendung der Ähnlichkeitsmechanik und Turbulenzforschung auf die Geschiebebewegung, *Mitt. Preuss. Vers. Wasserbau Schiffbau*, *26*, 5–24.

Sekine, M., and H., Kikkawa (1992), Mechanics of saltating grains, II, *J. Hydraul. Eng.*, *118*(4), 536–558.

Shimizu, Y., S. Giri, S. Yamaguchi, and J. Nelson (2009), Numerical simulation of duneflat bed transition and stage-discharge relationship with hysteresis effect, *Water Resour. Res.*, *45*, W04429, doi:10.1029/2008WR006830.

Swamee, P. K., and C. S. P. Ojha (1991), Drag coefficients and fall velocity of nonspherical particles, *J. Hydraul. Eng.*, *117*(5), 660–667.

Tritthart, M., B., Schober, and H., Habersack (2011), Non-uniformity and layering in sediment transport modelling. 1: Flume simulations, *J. Hydraul. Res.*, *49*(3), 325–334.

Van Rijn, L. C. (1984a), Sediment pick-up function, *J. Hydraul. Eng.*, *110*(10), 1494–1502.

Van Rijn, L. C. (1984b), Sediment transport, Part I: Bed load transport, *J. Hydraul. Eng.*, *110*, 1431–1456.

Van Rijn, L. C. (1993), Principles of sediment transport in rivers, estuaries and coastal seas, in *Aqua Publications*, Netherlands.

Wiberg, P. L., and J. D. Smith (1987), Calculations of the critical shear stress for motion of uniform and heterogeneous sediments, *Water Resour. Res.*, *23*(8), 1471–1480.

Wong, M., and G., Parker (2006), Reanalysis and correction of bedload relation of Meyer-Peter and Müller using their own database, *J. Hydraul. Eng.*, *132*(11), 1159–1168.

Wu, F. C., and Y. J. Chou (2003), Rolling and lifting probabilities for sediment entrainment, *J. Hydraul. Eng.*, *129*(2), 110–119.